RESEARCH ARTICLE

CLIMATE CHANGE

Recent global decline of CO$_2$ fertilization effects on vegetation photosynthesis

Songhan Wang[1,2], Yongguang Zhang[1,2,3]*, Weimin Ju[1,2], Jing M. Chen[1,4], Philippe Ciais[5], Alessandro Cescatti[6], Jordi Sardans[7,8], Ivan A. Janssens[9], Mousong Wu[1,2], Joseph A. Berry[10], Elliott Campbell[11], Marcos Fernández-Martínez[9], Ramdane Alkama[6], Stephen Sitch[12], Pierre Friedlingstein[13], William K. Smith[14], Wenping Yuan[15], Wei He[1,2], Danica Lombardozzi[16], Markus Kautz[17], Dan Zhu[5], Sebastian Lienert[18], Etsushi Kato[19], Benjamin Poulter[20], Tanja G. M. Sanders[21], Inken Krüger[21], Rong Wang[22], Ning Zeng[23,24], Hanqin Tian[25], Nicolas Vuichard[5], Atul K. Jain[26], Andy Wiltshire[12], Vanessa Haverd[27], Daniel S. Goll[5,28], Josep Peñuelas[7,8]

The enhanced vegetation productivity driven by increased concentrations of carbon dioxide (CO$_2$) [i.e., the CO$_2$ fertilization effect (CFE)] sustains an important negative feedback on climate warming, but the temporal dynamics of CFE remain unclear. Using multiple long-term satellite- and ground-based datasets, we showed that global CFE has declined across most terrestrial regions of the globe from 1982 to 2015, correlating well with changing nutrient concentrations and availability of soil water. Current carbon cycle models also demonstrate a declining CFE trend, albeit one substantially weaker than that from the global observations. This declining trend in the forcing of terrestrial carbon sinks by increasing amounts of atmospheric CO$_2$ implies a weakening negative feedback on the climatic system and increased societal dependence on future strategies to mitigate climate warming.

T errestrial ecosystems have accounted for more than half of the global carbon sink during the last six decades and have thus substantially mitigated climate warming (1). Global process-based models attribute part of the increasing land carbon sink (2) to the increase in vegetation productivity driven by the fertilization effect of increasing atmospheric CO$_2$ concentration (3), i.e., the CO$_2$ fertilization effect (CFE), a process that acts as a negative feedback in the climate system (4). First introduced by Keeling (5), the β factor generally is used to characterize the plant response to increasing CO$_2$ concentration. To compare the results between global analysis and experimental measurements, we used an approximation form of the original β (β = $\frac{\partial GPP}{\partial C_a}$) (6), which is defined as the relative increase in gross primary production (GPP) in response to a 100-ppm increase in atmospheric CO$_2$ concentration (C$_a$).

Increases of GPP originate from the direct acceleration of photosynthesis in response to the increased supply of CO$_2$ (7), but they are also modified by a suite of indirect responses, including water saving because of the reduced stomatal conductance under increasing atmospheric CO$_2$ concentrations (8, 9) and nutrient limitation (10). Enhanced GPP and net primary production (NPP) are commonly observed in field experiments, such as free-air CO$_2$ enrichment (FACE) experiments (7) and open-top chamber experiments (11), where ecosystems are exposed to elevated CO$_2$ in the range of two times ambient values, albeit with different response magnitudes across sites (7).

The fingerprint of CFE on the carbon and water cycles on global scales (3, 8) is, however, more elusive, given the covariation of atmospheric CO$_2$ with other environmental drivers of vegetation productivity. Elucidating this fingerprint of CFE is a scientific problem involving detection and attribution methods, requiring either statistical methods and long-term data such that effects of non-CFE drivers can be removed empirically (12, 13), or process-

based models with which CFE can be isolated by deliberate factorial simulations (14).

Process-based models of the terrestrial carbon cycle have indicated that CFE accounts for ~70% of the increasing global trend in foliar area, i.e., global greening (15), and up to 60% of the current terrestrial carbon sink (3). These models project that CFE will induce increased land carbon storage by the end of this century, despite opposing effects from climate change (3, 16). A cascade of uncertainties in projecting future land carbon storage arises from the responses of photosynthesis, NPP, and ecosystem carbon turnover times to increasing CO$_2$, especially in the presence of increasing limitations from nutrient and water availability. Therefore, accurately quantifying the temporal dynamics of CFE on GPP is essential for reducing the uncertainties of future land carbon storage and climate projections derived on the basis of Earth system models (4).

A study using the long-term CO$_2$ concentration measurements at the Barrow station (Alaska, 71°N) found that the sensitivity of the seasonal amplitude of atmospheric CO$_2$ to the increase in CO$_2$ concentration has decreased, which suggests a declining response of GPP to CO$_2$ at northern high latitudes (17). If such declining trends prevail across the globe, the terrestrial vegetation carbon sink response to increasing CO$_2$ will decrease, with important consequences for the global carbon budget and for the effort required from mitigation policies to meet future climate targets. For this reason, a comprehensive assessment of the temporal dynamics of CFE on global GPP is timely as a first step to understand the impacts of CFE on the trends of the land carbon sinks. We used three long-term satellite datasets collected during 1982 to 2015: a recently developed vegetation index (NIR$_V$) (18) from the Advanced Very High Resolution Radiometer (AVHRR NIR$_V$), the fusion of NIR$_V$ from AVHRR and the Moderate Resolution Imaging Spectroradiometer (AVHRR+MODIS NIR$_V$), and the fusion of NIR$_V$ and sun-induced chlorophyll fluorescence (SIF) (19) (NIR$_V$+SIF), which are proxies for GPP (hereafter, satellite GPP proxies) (supplementary text S1 and figs. S1 to S5) (20). We also corroborated our findings using long-term GPP time series from

[1]International Institute for Earth System Science, Nanjing University, Nanjing, Jiangsu 210023, China. [2]Jiangsu Provincial Key Laboratory of Geographic Information Technology, Key Laboratory for Land Satellite Remote Sensing Applications of Ministry of Natural Resources, School of Geography and Ocean Science, Nanjing University, Nanjing, Jiangsu 210023, China. [3]Huangshan Park Ecosystem Observation and Research Station, Ministry of Education, Huangshan, China. [4]Department of Geography and Planning, University of Toronto, Toronto, Ontario, Canada. [5]Laboratoire des Sciences du Climat et de l'Environnement, CEA CNRS UVSQ, Gif-sur-Yvette, France. [6]European Commission, Joint Research Centre (JRC), Ispra, Italy. [7]CSIC, Global ecology Unit CREAF-CSIC-UAB, Bellaterra 08193, Catalonia, Spain. [8]CREAF, Cerdanyola del Vallès 08193, Catalonia, Spain. [9]Department of Biology, Centre of Excellence PLECO (Plant and Vegetation Ecology), University of Antwerp, Wilrijk, Belgium. [10]Department of Global Ecology, Carnegie Institution for Science, Stanford, CA 94305, USA. [11]Sierra Nevada Research Institute, University of California, Merced, CA 95343, USA. [12]College of Life and Environmental Sciences, University of Exeter, Exeter, UK. [13]College of Engineering, Mathematics and Physical Sciences, University of Exeter, Exeter, UK. [14]School of Natural Resources and the Environment, University of Arizona, Tucson, AZ, USA. [15]School of Atmospheric Sciences, Center for Monsoon and Environment Research, Sun Yat-Sen University, Guangzhou, China. [16]Terrestrial Sciences Section, National Center for Atmospheric Research, Boulder, CO, USA. [17]Forest Research Institute Baden-Württemberg, Freiburg, Germany. [18]Climate and Environmental Physics, Physics Institute, and Oeschger Centre for Climate Change Research, University of Bern, Bern, Switzerland. [19]Institute of Applied Energy, Tokyo, Japan. [20]NASA Goddard Space Flight Center, Greenbelt, MD 20771, USA. [21]Thünen Institute of Forest Ecosystems, Alfred-Möller-Str. 1, 16225 Eberswalde, Germany. [22]Department of Environmental Science and Engineering, Fudan University, Shanghai, 200433, China. [23]Department of Atmospheric and Oceanic Science, University of Maryland, College Park, MD 20742, USA. [24]LASG, Institute of Atmospheric Physics, Chinese Academy of Science, Beijing 100029, China. [25]International Center for Climate and Global Change Research, School of Forestry and Wildlife Sciences, Auburn University, Auburn, AL, USA. [26]Department of Atmospheric Sciences, University of Illinois, 105 South Gregory Street, Urbana, IL 61801-3070, USA. [27]CSIRO Oceans and Atmosphere, Canberra, ACT 2601, Australia. [28]Institute of Geography, University of Augsburg, Augsburg, Germany.
*Corresponding author. Email: yongguang_zhang@nju.edu.cn

eddy covariance (EC) flux towers, from a light use efficiency (LUE) model (21), and from an ensemble of terrestrial carbon cycle models (TRENDY v6, trends and drivers of the regional scale sources and sinks of carbon dioxide) (14).

Global temporal trend of β from observations and models

Linear and nonlinear multiple regression approaches were used to estimate β from satellite GPP proxies at each pixel across the globe (12, 13, 20). Pixels with large land-cover changes were excluded from the analyses (supplementary text S2 and fig. S6). The global median β during 1982 to 2015 was 16.1 ± 11.5% 100 ppm^{-1} (fig. S7), consistent with the FACE experiments (7), which on average suggested a 15.5% increase in light-saturated photosynthesis per 100 ppm CO_2. Results showed that the estimated β values for different vegetation physiology and biome types were also aligned with experimental results (7), e.g., the β values of C_4 plants were much smaller than those of C_3 plants (supplementary text S3 and fig. S8). We next calculated the time series of β with 15-year moving windows during 1982 to 2015 and found that β significantly decreased at a rate of −0.92 ± 0.12% 100 ppm^{-1} year^{-1} ($p < 0.01$) (Fig. 1A). This decrease was also evident after excluding the crop areas (fig. S9). Compared with the global median of the declining trend in β, grasslands and plants in cold climate zones exhibited a larger declining trend of β, whereas the β trends of shrubs and plants in tropical areas were slightly lower; nevertheless, the decreases in β across all the climate zones and vegetation types were notable (fig. S10). Across the global terrestrial areas, β

Fig. 1. Declining trend of global β. Temporal dynamics of β for three satellite GPP proxies with 15-year moving windows during 1982 to 2015. The gray area indicates 1 SD on either side of the mean. The trend and statistical significance (p value) of the β time series were estimated using the Mann-Kendall test. (**B**) (Left) The histogram distribution of β across all pixels in two 15-year periods. β was the average of these three satellite GPP proxies. (Right) Boxes represent the interquartile ranges of the β values (solid lines represent medians), and whiskers extend to one times the interquartile range. Median β values for these two periods and their SDs are shown at the top of the graph. The SDs in (A) and (B) were calculated based on the data in the range of the y axis. Only the range of [−10, 50] is shown for visualization purposes. The asterisk indicates a significantly different β between these two periods, on the basis of a two-sample Kolmogorov-Smirnov test at $p < 0.01$.
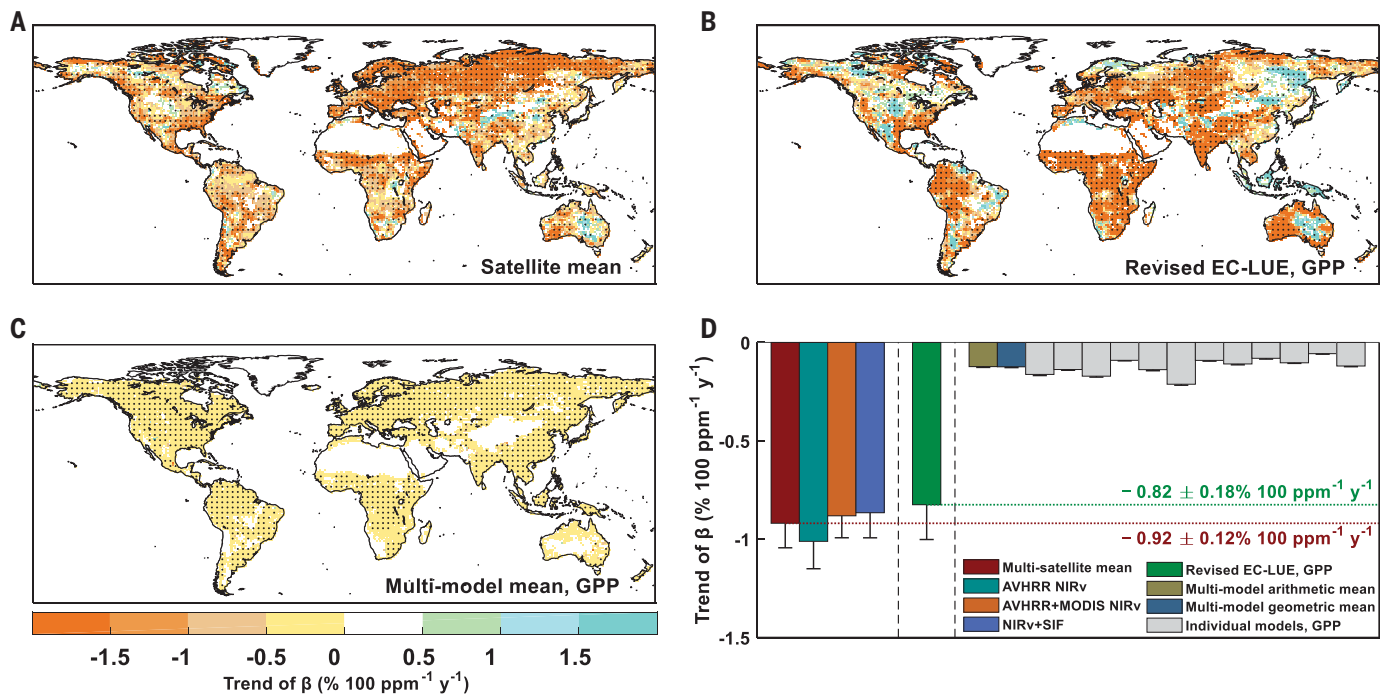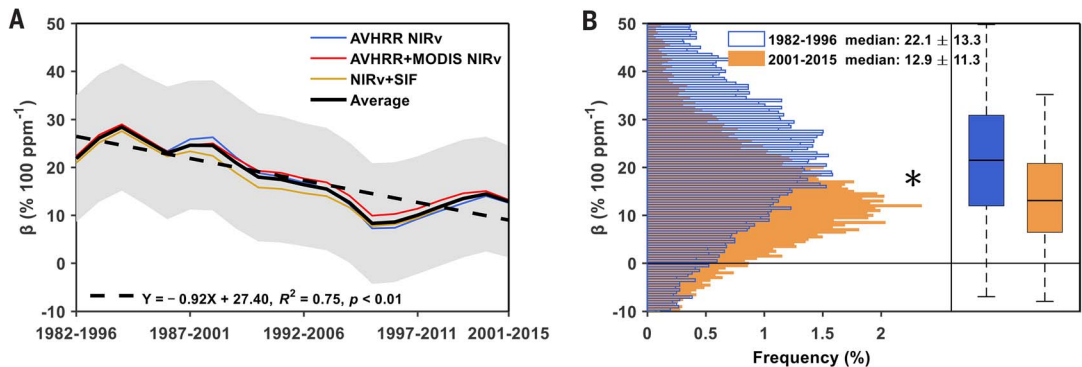

Fig. 2. Global declining trend of β. Spatial patterns of trends in β derived from three datasets using 15-year moving windows, reported as the percentage per 100 ppm per year. (**A**) Means from three satellite GPP proxies. (**B**) The revised EC-LUE GPP. (**C**) Multimodel mean GPP determined from the TRENDY v6 ensemble. All datasets are from 1982 to 2015. The Mann-Kendall test was used to estimate the trend of β pixel by pixel, and the regions with black dots indicate significant trends ($p < 0.05$). The pixel size is 1°. (**D**) Mean declining trend of β from different datasets. The error bars represent SEs.

significantly declined from 22.1 ± 13.3% 100 ppm^{-1} during 1982 to 1996 to 12.9 ± 11.3% 100 ppm^{-1} during 2001 to 2015 (Fig. 1B).

We also found a robust decrease in β when we used another satellite NIRv time series (fig. S11), various land cover change masks (fig. S12), different window lengths (supplementary text S4 and fig. S13), various combinations of explanatory variables (supplementary text S5 and figs. S14 and S15), and different definitions of growing seasons (fig. S16) and when we included the consideration of seasonal precipitation (supplementary text S6 and fig. S17). After considering the uncertainties from original satellite data and from the methods, the global β estimated from satellite GPP proxies during 2001 to 2015 was still significantly lower than that during 1982 to 1996 (supplementary text S7 and figs. S18 and S19). To verify whether the trend of β was an artefact of our regression method, we also estimated the temporal dynamics of β using the optimal fingerprint attribution method (supplementary text S8) and again found that the declining trend of β was significant (fig. S20). Altogether, these results based on satellite observations of GPP proxies suggest a significant declining trend in the response of GPP to increasing atmospheric CO_2.

To further assess the decreases in β inferred from satellite GPP proxies, we used other independent datasets: (i) the GPP time series derived from the revised EC-LUE model (21) (which also accounted for the direct CO_2 effects on LUE); (ii) satellite-based leaf area index (LAI) time series; (iii) multiyear GPP estimations from 22 EC flux sites (table S4); and (iv) a global long-term GPP dataset from the Carbon Cycle Data Assimilation System (CCDAS) (supplementary text S9 to S12). We also found a significant declining trend of β on the basis of the revised EC-LUE GPP, with a rate of −0.82 ± 0.18% 100 ppm^{-1} year^{-1} (fig. S21), similar to the estimates from satellite GPP

proxies. However, the result from satellite-based LAI showed a smaller declining rate of β (−0.59 ± 0.11% 100 ppm^{-1} year^{-1}) (fig. S22). This divergence suggested that the decrease in β was likely due to two factors: the direct effect on foliar physiology and the indirect effect on LAI. The former refers to the CO_2-induced stimulation of carboxylation per unit leaf area, whereas the latter depicts the increased carbon sequestration used for leaf area expansion. The smaller declining β trend from satellite LAI suggested that these two effects were both relevant for the full description of the global decreases in the CO_2 effect on GPP. Ground GPP estimates from EC flux sites also confirmed our findings, by indicating an average declining rate of β at −0.70% 100 ppm^{-1} year^{-1}, which was comparable to the results from satellite GPP proxies around these sites (fig. S23). On the basis of the CCDAS GPP, a data–model fusion product constrained by atmospheric CO_2 observations and which is independent from satellite data, we also found a declining β trend at a rate of −0.62% 100 ppm^{-1} year^{-1} (fig. S24). The overall consistency between various remote-sensing data, ground measurements, and a carbon assimilation system suggests that the global decline of β is robust and coherent across multiple, independent observations.

## Spatial pattern of the temporal trend of β across the globe

The geographic distribution of the temporal trends of β from satellite GPP proxies (Fig. 2A) revealed that β decreased in ~86% of global lands (fig. S25, A to C). Areas with declining β spanned over most of the globe. By contrast, increasing β was found in some limited regions of Southeast Asia, east Australia, and North America (Fig. 2, A and B). These increasing β trends are likely driven by an intensification of management in croplands (i.e., irrigation and fertilization) or related to in-

creasing atmospheric nutrients deposition in recent years (fig. S33). We also observed similar spatial patterns for β trends calculated using both 10-year and 17-year moving windows (fig. S26). Overall, the decreases of β in tropical areas were smaller, whereas cold regions had a slightly stronger declining trend (figs. S10A and S25, A to C). The latter may be because the declining signals of β in northern high latitudes include both the indirect effects on LAI and the direct effect on foliar physiology, whereas those in warmer climates include only the physiological effect, given that LAI in some tropical humid regions may already be close to saturation. Results of the satellite LAI confirmed this interpretation by suggesting a larger reduction of β in colder northern regions than in warmer climates (fig. S25, E and F). Similar declines in β were obtained from the revised EC-LUE GPP, which covered ~74% of the global terrestrial area (Fig. 2B). In general, all datasets indicated that β has been declining in most global lands and across various vegetation types and climate zones.

We also investigated whether an ensemble of state-of-the-art carbon cycle models (14) was able to reproduce these observed global declines of β on GPP. We used results from 12 models that contributed to the TRENDY v6 ensemble to calculate β (20) (supplementary text S13). For each model, we extracted the differences in simulated GPP between S1 (time-varying CO_2 only) and S0 (constant CO_2) scenarios, which represented the CO_2 effect on vegetation productivity. These models predicted a negative trend in β, both for the multimodel mean and for the individual one, but the declining rate was clearly lower than that derived from satellite GPP proxies and with no evident spatial variations (Fig. 2C and fig. S27). Grouping the estimates of CFE trends, we found that the global β declined at a rate of −0.92 ± 0.12% 100 ppm^{-1} year^{-1} for satellite GPP proxies and only −0.12 ± 0.01% 100 ppm^{-1}

Fig. 3. Relationship between the residual trend of β and foliar nutrient concentrations. Results for foliar N (**A**) and foliar P (**B**) concentrations after accounting for site mean annual air temperature, and mean annual precipitation from 3846 samples on the basis of a spatial mixed-effects model. Model performance and results are presented in table S5. Data are classified into 50 bins for clear visualization on the basis of foliar N or P concentrations. The red dots represent the means for each bin, and the blue lines

represent the SDs of the means. The gray dots represent the raw individual samples, and black lines represent the linear regressions of these gray dots. The correlation coefficients (r) and p values were calculated on the basis of the raw data (n = 3846).
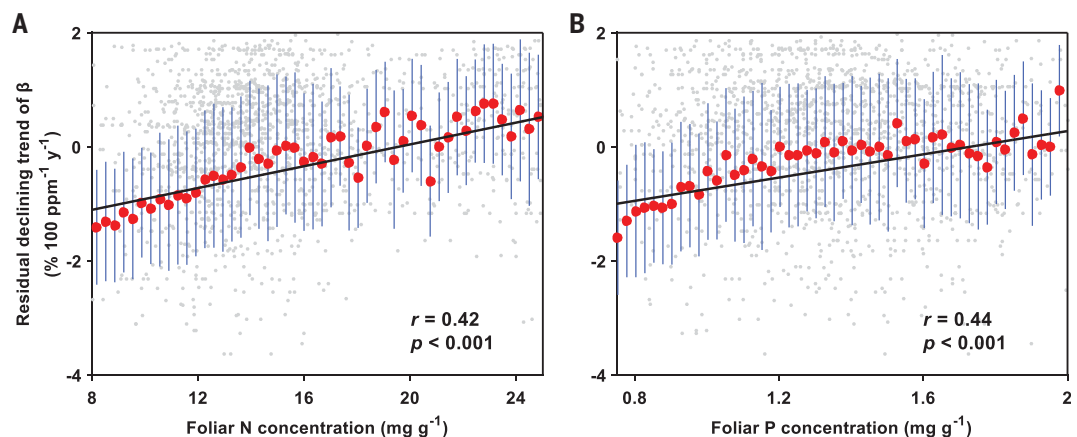
year^{-1} for TRENDY GPP (Fig. 2D). β trends of individual models were variable, from −0.06 to −0.21% 100 ppm^{-1} year^{-1} (fig. S28), but all of them were lower than that from satellite GPP proxies. Given that we defined β as the percent increase in GPP per 100-ppm increase in CO_2 and that the S1 simulations solely considered the CO_2 effect, the smaller decreases in β from TRENDY GPP were likely caused by the saturating physiological response of GPP to CO_2 (22), without adequately capturing the concurrent emergence of other limiting factors driven by the changing environmental conditions. We also used GPP from the TRENDY S2 and S3 scenarios to estimate the trends in β by using the regression approaches (20). The temporal trends of β remained unaltered, with a value of approximately −0.12 ± 0.12% 100 ppm^{-1} year^{-1} for both TRENDY S2 and S3 simulations (fig. S29). These results highlight that the ongoing strong decrease in β inferred from satellite datasets is probably underestimated by TRENDY models.

Possible mechanisms accounting for the declining β

Two possible non–mutually exclusive hypotheses were proposed to account for the declining β and to explain why TRENDY models failed to adequately replicate the magnitude of this decline: (i) the increasing constraints on vegetation productivity from emerging nutrient limitations and imbalances that were not adequately represented in models and (ii) current models underestimated the sensitivity of terrestrial GPP to changes in water availability.

The first hypothesis relates to the possible effect of the growing limitation of key nutrients, including nitrogen (N) and phosphorus (P). Using 410 groups of ground-based foliar N and P observations (supplementary text S14 and fig. S30), we found a general decrease in foliar N and P concentrations, with mean values of −0.24 ± 0.06% year^{-1} and −0.55 ± 0.06% year^{-1}, respectively (fig. S31, A and B). Our findings are consistent with a recent study suggesting a general global pattern of decreasing foliar N concentration (23) and with many examples of local to regional decreases in foliar N and P concentrations (24, 25). Enhanced GPP from the increasing atmospheric CO_2 concentrations, leading to larger NPP and higher nutrient demands by plants, may partly explain the observed declines of foliar N and P concentrations. Concurrently, these decreases in key foliar nutrients may impose limitations on GPP and thereby limit β. To test this hypothesis, we applied a linear spatial mixed-effects model (table S5) to investigate the relationship between the trend of β and foliar N or P concentrations (supplementary text S14 and fig. S32). After accounting for the trends in β explained statistically by mean annual air temperature and mean annual precipitation, we found clear positive correlations between the residual declining trends of β with both foliar N and P concentrations across European forests (Fig. 3). These results suggested that vegetation with lower foliar nutrient concentrations generally showed larger declines in β, therefore supporting our hypothesis of a role for nutrient limitation in the temporal dynamics of β.

This phenomenon was also verified from global trends in atmospheric N and P depositions, which suggested that areas with decreasing atmospheric nutrient supplies probably had larger decreases in β (such as Europe and Siberia) and vice versa (such as East Asia) (fig. S33). This may be because vegetation in areas with declining nutrient supplies from atmospheric depositions tend to have larger N and P limitations on GPP. Moreover, the increases of N and P depositions in some regions of East Asia may explain the increasing trend of β in these areas (Figs. 2A and fig. S33). The ongoing decreases in foliar nutrients might constrain the plant photosynthetic capacity and result in the decline of β, which might not have been adequately represented in current models (supplementary text S14). Regarding this aspect, the models that included C-N cycle interactions to emulate nutrient constraints exhibited a larger declining rate of β (fig. S34), partly confirming this interpretation. The role of N limitation on β has been widely suggested by experimental evidence (10, 26, 27), model analyses (28), and synthesis reviews (29, 30), all of which have been consistent with our analyses. Our finding regarding P limitation was also consistent with FACE experiments, which demonstrated that insufficient P availability generally had negative impacts on β (31). Furthermore, as foliar P:N ratios positively correlated with plant net photosynthesis and growth (32), the decreasing foliar P:N ratios in European forests (fig. S31C) suggested a worsening nutrient imbalance that may partly account for the observed decline in β.

The second hypothesis to explain the divergence of the β trend between the TRENDY models and the satellite-derived estimates stated that these models underestimated the sensitivity of GPP to water availability, because the coupling between water and carbon in models is underestimated (33). To test this hypothesis, we analyzed the sensitivity of satellite GPP
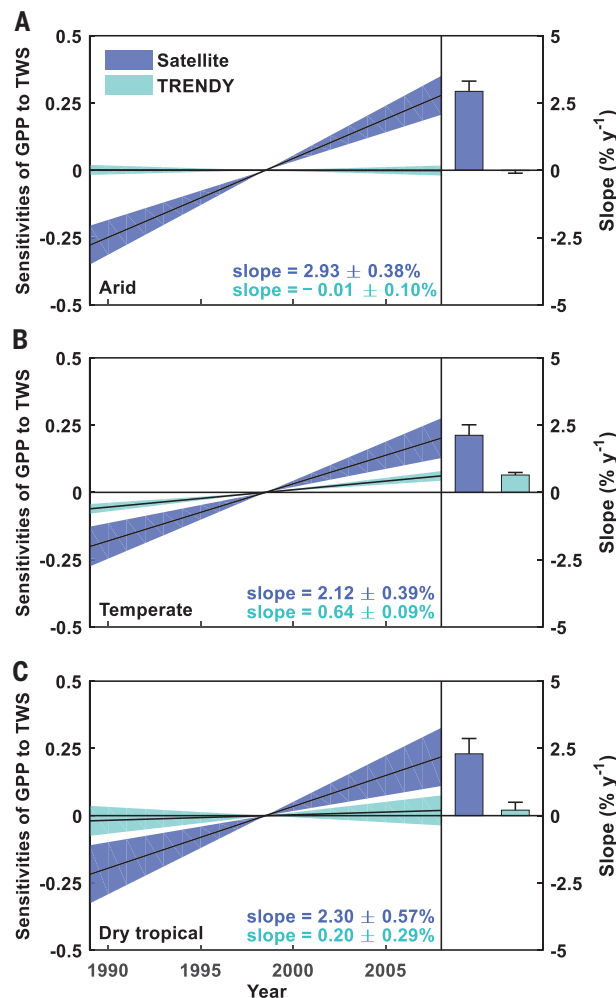

Fig. 4. Sensitivities of GPP to TWS. The changes in satellite GPP proxies or TRENDY GPP per unit change in TWS were estimated for arid (**A**), temperate (**B**), and dry tropical (**C**) climate zones using a moving window of 15 years. The sensitivity time series have been standardized. The solid lines in the left panels represent the linear regressions. The shaded areas represent the SEs. The bars and error bars in the right panels represent the slopes and their SEs, respectively.

proxies and TRENDY GPP to water availability using a moving window of 15 years (supplementary text S15). We used the terrestrial water storage (TWS) data to represent the availability of water to plants and selected arid, temperate, and dry tropical climate zones as the research areas (fig. S35), as the GPP in these zones was found to be highly sensitive to TWS (fig. S36). We observed that the sensitivity of GPP to TWS was relatively constant across these three zones for the multimodel mean of the TRENDY GPP, whereas the TWS sensitivities derived from satellite GPP proxies exhibited significantly increasing trends for arid (2.93 ± 0.38% year^{-1}), temperate (2.12 ± 0.39% year^{-1}), and dry tropical (2.30 ± 0.57% year^{-1}) ecosystems (Fig. 4). In temperate and dry tropical areas, the majority of models exhibited divergent results compared to satellite GPP proxies, and almost all of them largely underestimated the GPP sensitivities to TWS in arid areas (fig. S37). The decreases in β were larger in the regions where the increases of TWS sensitivities were higher (fig. S38). These strongly divergent sensitivities between satellite GPP proxies and TRENDY GPP were also confirmed when using various TWS products (20) (supplementary text S15 and fig. S39) and when using a shorter moving window (fig. S40).

This finding implies that GPP and consequently land carbon uptake are more sensitive to the variations in water availability than assumed by the TRENDY models, as previously suggested by several recent studies (34, 35). Moreover, a recent study showed that the CFE of grasslands could be reduced under drier conditions (36). The relationship between drought stress and CFE is complex and ecosystem specific and may be affected by the total annual rainfall as well as rainfall seasonality. It was shown, for instance, in 19 grasslands experiments that the annual CFE was negated when spring precipitation became too low (37). Field experiments also support our results by suggesting that the CFE on vegetation productivity is at least partly limited by water availability (38). The significant increases in the GPP sensitivities to TWS may thus partly explain the decreases of β in arid, temperate, and dry tropical climate zones.

From a theoretical perspective, the global declines of CFE may result from several factors. First, given that the CO_2-induced photosynthesis stimulation at the leaf level is scaled up to the canopy level through LAI (39, 40), the declining β on the basis of satellite LAI (fig. S22) could partly explain the global decreases of the GPP response to CO_2. Consistent with our findings, a recent study using the FACE experiments on mature forests found a relatively low CO_2 effect on GPP (41), possibly because the LAI of these forests did not change much (39). Second, the CO_2 effect on photo-

synthesis at the leaf level involves both the stimulation of carboxylation and increases in water use efficiency (WUE). The former may possibly be regulated by the foliar key nutrients (N and P), and the latter is related to the water availability. According to the progressive N limitation theory, the soil N availability for plant growth may be expected to diminish over time (42), possibly leading to the observed global decreases in β. A recent study using carbon isotope measurements revealed diminishing CO_2-induced WUE gains across global forests (43), which supported our findings of the effects of water supply limitation on CFE and could partly explain the global declines in β. Moreover, complex interactive effects between nutrients and water supply may also have impacts on CFE. For example, low soil water supply could possibly strengthen the nutrient constraints on CFE through limiting nutrient decomposition and diffusion in soils (38). Our further analysis using model simulations showed that the GPP trends have clear reductions in arid areas, once the interactions between N limitation and climate constraints are considered, supporting this hypothesis (fig. S41B and supplementary text S16). Nevertheless, an excess of N fertilizer may result in a reduction in the soil water and therefore possibly lead to drought stress (44). Regarding this aspect, our analysis also highlights the need for future efforts to better understand the complex interactions between nutrients, water, and CO_2 effects on vegetation from a climate change perspective. Additional mechanisms (e.g., plant acclimation or changes in plant species over time) may also explain the observed global decrease in CFE (supplementary text S17).

Conclusion

Our analyses showed a significant and spatially extensive decline in β, which implies a substantial reduction of the positive effects of increasing atmospheric CO_2 on terrestrial carbon uptake. A recent study suggested that the CO_2 effect on the carbon cycle in tropical regions (3) might be counteracted by impacts from climate-driven changes (45), in agreement with our findings. Although still under debate, the possible increasing trend of the airborne fraction of anthropogenic CO_2 may imply a saturation of the CO_2 sinks from land and oceans (46–49), which may be partly caused by the global decline in CFE. Current carbon cycle models also exhibit such global decreases in β but fail to adequately detect the sharp declining trend that we identified from satellite data. This divergence between observations and process-based models possibly originates from the models' limitations in adequately representing the emerging decline in key foliar nutrient concentrations and the increasing constraints of water limitations on vegetation

productivity. Ultimately, these results indicate that terrestrial photosynthesis may not increase as much as models project, possibly reducing the potential of land-based climate mitigation, further accelerating global warming and exacerbating the efforts required for meeting climate targets. Our findings also highlight the need for better characterizations of the biogeochemical and hydrological effects on vegetation in current carbon cycle models to produce more robust projections of the terrestrial carbon budget for the next decades.

REFERENCES AND NOTES

1. P. Friedlingstein et al., Earth Syst. Sci. Data 11, 1783–1838 (2019).
2. A. P. Ballantyne, C. B. Alden, J. B. Miller, P. P. Tans, J. W. White, Nature 488, 70–72 (2012).
3. D. Schimel, B. B. Stephens, J. B. Fisher, Proc. Natl. Acad. Sci. U.S.A. 112, 436–441 (2015).
4. P. Friedlingstein et al., J. Clim. 27, 511–526 (2014).
5. C. D. Keeling, "The carbon dioxide cycle. Reservoir models to depict the exchange of atmospheric carbon dioxide with the oceans and land plants" in Chemistry of the Lower Atmosphere, S. I. Rasool, Ed. (Plenum, 1973), pp. 251–329.
6. R. Bacastow, C. D. Keeling, "Atmospheric carbon dioxide and radio-carbon in the natural carbon cycle. II: Changes from A.D. 1700 to 2070 as deduced from a geochemical model" in Carbon in the Biosphere, G. M. Woodwell, E. V. Pecan, Eds. (Atomic Energy Commission, 1973), pp. 86–136.
7. E. A. Ainsworth, A. Rogers, Plant Cell Environ. 30, 258–270 (2007).
8. T. F. Keenan et al., Nature 499, 324–327 (2013).
9. J. A. Morgan et al., Nature 476, 202–205 (2011).
10. P. B. Reich et al., Nature 440, 922–925 (2006).
11. W. I. Dieleman et al., Glob. Change Biol. 18, 2681–2693 (2012).
12. S. Piao et al., Glob. Change Biol. 19, 2117–2132 (2013).
13. W. Kolby Smith et al., Nat. Clim. Chang. 6, 306–310 (2016).
14. S. Sitch et al., Biogeosciences 12, 653–679 (2015).
15. Z. Zhu et al., Nat. Clim. Chang. 6, 791–795 (2016).
16. P. M. Cox et al., Nature 494, 341–344 (2013).
17. J. Peñuelas et al., Nat. Ecol. Evol. 1, 1438–1445 (2017).
18. G. Badgley, C. B. Field, J. A. Berry, Sci. Adv. 3, e1602244 (2017).
19. L. Guanter et al., Proc. Natl. Acad. Sci. U.S.A. 111, E1327–E1333 (2014).
20. Materials and methods are available as supplementary materials.
21. W. Yuan et al., Sci. Adv. 5, eaax1396 (2019).
22. M. G. De Kauwe, T. F. Keenan, B. E. Medlyn, I. C. Prentice, C. Terrer, Nat. Clim. Chang. 6, 892–893 (2016).
23. J. M. Craine et al., Nat. Ecol. Evol. 2, 1735–1744 (2018).
24. M. Jonard et al., Glob. Change Biol. 21, 418–430 (2015).
25. K. K. McLauchlan et al., Sci. Rep. 7, 7856 (2017).
26. R. E. McMurtrie et al., Funct. Plant Biol. 35, 521–534 (2008).
27. R. J. Norby, J. M. Warren, C. M. Iversen, B. E. Medlyn, R. E. McMurtrie, Proc. Natl. Acad. Sci. U.S.A. 107, 19368–19373 (2010).
28. Global Biogeochem. Cycles 9, 407–437 (1995).
29. H. Mooney, B. G. Drake, R. Luxmore, W. Oechel, L. Pitelka, Bioscience 41, 96–104 (1991).
30. A. D. McGuire, J. M. Melillo, L. A. Joyce, Annu. Rev. Ecol. Syst. 26, 473–503 (1995).
31. C. Terrer et al., Nat. Clim. Chang. 9, 684–689 (2019).
32. J. Peñuelas et al., Nat. Commun. 4, 2934 (2013).
33. V. Humphrey et al., Nature 560, 628–631 (2018).
34. P. B. Reich et al., Nature 562, 263–267 (2018).
35. J. K. Green et al., Science 565, 476–479 (2019).
36. W. Obermeier et al., Nat. Clim. Chang. 7, 137–141 (2017).
37. M. J. Hovenden et al., Nat. Plants 5, 167–173 (2019).
38. P. B. Reich, S. E. Hobbie, T. D. Lee, Nat. Geosci. 7, 920–924 (2014).
39. Y. Luo, S. Niu, Nature 580, 191–192 (2020).
40. Q. Li et al., Biogeosciences 15, 6909–6925 (2018).
41. M. Jiang et al., Nature 580, 227–231 (2020).
42. Y. Luo et al., Bioscience 54, 731–739 (2004).
43. M. A. Adams, T. N. Buckley, T. L. Turnbull, Nat. Clim. Chang. 10, 466–471 (2020).
44. E. C. da Silva, R. Nogueira, M. A. da Silva, M. B. de Albuquerque, Plant Stress 5, 32–41 (2011).
45. J. Liu et al., Science 358, eaam5690 (2017).
46. J. G. Canadell et al., Proc. Natl. Acad. Sci. U.S.A. 104, 18866–18870 (2007).

47. M. Raupach, J. Canadell, C. Le Quéré, *Biogeosciences* **5**, 1601–1613 (2008).
48. W. Knorr, *Geophys. Res. Lett.* **36**, L21710 (2009).
49. M. R. Raupach *et al.*, *Biogeosciences* **11**, 3453–3475 (2014).

SUPPLEMENTARY MATERIALS
science.sciencemag.org/content/370/6522/1295/suppl/DC1
Materials and Methods
Supplementary Text S1 to S18
Figs. S1 to S47
Tables S1 to S5
References (*50–138*)
MDAR Reproducibility Checklist

31 March 2020; accepted 23 October 2020
10.1126/science.abb7772

Recent global decline of CO$_2$ fertilization effects on vegetation photosynthesis

Songhan Wang, Yongguang Zhang, Weimin Ju, Jing M. Chen, Philippe Ciais, Alessandro Cescatti, Jordi Sardans, Ivan A. Janssens, Mousong Wu, Joseph A. Berry, Elliott Campbell, Marcos Fernndez-Martnez, Ramdane Alkama, Stephen Sitch, Pierre Friedlingstein, William K. Smith, Wenping Yuan, Wei He, Danica Lombardozzi, Markus Kautz, Dan Zhu, Sebastian Lienert, Etsushi Kato, Benjamin Poulter, Tanja G. M. Sanders, Inken Krger, Rong Wang, Ning Zeng, Hanqin Tian, Nicolas Vuichard, Atul K. Jain, Andy Wiltshire, Vanessa Haverd, Daniel S. Goll, and Josep Peuelas

A decline in the carbon fertilization effect

One source of uncertainty in climate science is how the carbon fertilization effect (CFE) will contribute to mitigation of anthropogenic climate change. Wang *et al.* explored the temporal dynamics of CFE on vegetation photosynthesis at the global scale. There has been a decline over recent decades in the contribution of CFE to vegetation photosynthesis, perhaps owing to the limiting effects of plant nutrients such as nitrogen and phosphorus. This declining trend has not been adequately accounted for in carbon cycle models. CFE thus has limitations for long-term mitigation of climate change, and future warming might currently be underestimated.

Science, this issue p. 1295

View the article online
https://www.science.org/doi/10.1126/science.abb7772
Permissions
https://www.science.org/help/reprints-and-permissions

Use of this article is subject to the Terms of service